

1 Extreme oxygen isotope zoning in garnet and zircon from a
2 metachert block in mélangé reveals metasomatism at the peak of
3 subduction metamorphism

4 **F. Zeb Page¹, Emilia M. Cameron^{1,2}, Clara Margaret Flood¹, Jeffrey W. Dobbins¹, Michael**
5 **J. Spicuzza², Kouki Kitajima², Ariel Strickland², Takayuki Ushikubo^{2***}, Christopher G.**
6 **Mattinson³, and John W. Valley²**

7 *¹ Geology Department, Oberlin College, Oberlin, Ohio 44074, USA*

8 *² WiscSIMS, Department of Geoscience, University of Wisconsin -Madison, Wisconsin 53706,*
9 *USA*

10 *³Department of Geological Sciences, Central Washington University, Ellensburg, Washington*
11 *98926*

12 **** Present Address: Kochi Institute for Core Sample Research, JAMSTEC 200 Monobe-otsu,*
13 *Nankoku, Kochi 783-8502 Japan*

14

15

16 Post-Review revision

17 April 17, 2019

18

19 **ABSTRACT**

20 A tectonic block of garnet quartzite in the amphibolite-facies mélange of the Catalina
21 Schist (Santa Catalina Island, California, USA) records the metasomatic pre-treatment of high-
22 $\delta^{18}\text{O}$ sediments as they enter the subduction zone. The block is primarily quartz, but contains two
23 generations of garnet that record extreme oxygen isotope disequilibrium and inverse
24 fractionations between garnet cores and matrix quartz. Rare mm-scale garnet crystals record
25 prograde zonation patterns, whereas more abundant $\sim 200\text{-}\mu\text{m}$ diameter crystals have the
26 same composition as rims on the larger garnets. Garnets of both generations have high $\delta^{18}\text{O}$
27 cores (20.8-26.3‰, VSMOW) that require an unusually high- $\delta^{18}\text{O}$ protolith, and lower- $\delta^{18}\text{O}$,
28 less variable rims (10.0-11.2‰). Matrix quartz values are homogeneous (13.6‰). Zircon
29 crystals contain detrital cores ($\delta^{18}\text{O} = 4.7\text{-}8.5\text{‰}$, $124.6 \pm 1.4\text{-}2.9$ Ma), with characteristic igneous
30 trace-element composition likely sourced from arc-volcanics, surrounded by zircon with
31 metamorphic age (115.1 ± 2.5 Ma) and trace-element compositions that suggest growth in the
32 presence of garnet. Metamorphic zircon decreases in $\delta^{18}\text{O}$ from near-core (24.1‰) to rim
33 (12.4‰), in equilibrium with zoned garnets.

34 Collectively, the data document the subduction of a mixed high- $\delta^{18}\text{O}$ siliceous
35 ooze/volcanic ash protolith reaching temperatures of 550-625 °C prior to the nucleation of small
36 garnets without influence from external fluids. Metasomatism is recorded in rims of both garnet
37 and zircon populations as large volumes of broadly homogeneous subduction fluids stripped
38 matrix quartz of its extremely high oxygen isotope signature. Zoned garnet and zircon in high-
39 $\delta^{18}\text{O}$ subducted sediments offer a detailed window into subduction fluids.

40

41

42 INTRODUCTION

43 The nature and timing of mass transfer between the subducting plate and the sub-arc
44 mantle is critical to our understanding of crustal formation at convergent margins and its
45 geochemical signatures. Chemical and mechanical hybridization within subduction mélange
46 plays an important role in these processes (e.g., Bebout and Penniston-Dorland, 2016), giving
47 rise to models suggesting that partial melting of diapirs of hybridized mélange rocks are
48 responsible for the classic trace element signature of arc rocks (Marschall and Schumacher,
49 2012) and the diversity of magma series found at convergent margins (Cruz-Uribe et al., 2018).
50 Adding to these complications is the recent discovery that some sediments have entered the
51 mantle and melted without mixing or hybridization, preserving extreme oxygen isotope
52 signatures of surface weathering in their neofomed igneous zircon (Spencer et al., 2017). If
53 subducted sediment can regularly carry its characteristically enriched oxygen isotope signature
54 ($\delta^{18}\text{O} = \sim 7 - 42\text{‰}$, VSMOW [Vienna standard mean ocean water]; Kolodny and Epstein, 1976;
55 Eiler et al., 2001; Payne et al, 2015) into the mantle ($\delta^{18}\text{O}_{\text{O1}} = 5.1\text{‰}$, Eiler et al., 2000), it is
56 surprising that oxygen isotope variability within the subarc mantle is so subtle and challenging to
57 measure (Eiler et al., 1998). A solution to this discrepancy may be found in the fluid
58 metasomatism of subducted sediments.

59 The first and perhaps most dramatic illustrations of a high degree of fluid flow within
60 subduction mélange were studies of the oxygen isotope ratios of quartz and carbonate in veins
61 within the Catalina Schist subduction complex (California, USA) suggesting km-scale oxygen
62 isotope homogenization driven by large fluid fluxes (Bebout and Barton, 1989; Bebout, 1991).
63 Over the last quarter century, the Catalina Schist has served as a laboratory for the study of
64 subduction mélange, with numerous studies detailing fluid metasomatism and mechanical

65 mixing processes in the subduction channel by means of stable isotopes (e.g., Bebout, 1991;
66 Penniston-Dorland et al., 2012), major and trace elements (e.g., Sorenson and Barton, 1987;
67 Hickmott et al., 1992; Penniston-Dorland et al., 2014) and radiogenic isotopes (King et al.,
68 2006).

69 The in-situ analysis of oxygen isotopes in garnet is a powerful tool with which to
70 decipher complex or extremely subtle fluid histories and tie them to the metamorphic record. In
71 rocks that have experienced significant metasomatism, the extremely slow intragranular
72 diffusion of oxygen in garnet allows it to preserve a robust geochemical record through all but
73 the hottest and longest of metamorphic events (Vielzeuf et al., 2005). Oxygen isotope variability
74 in garnets from eclogite has illustrated signals of infiltration by mantle (Russell et al., 2013) and
75 supracrustal (e.g., Page et al., 2014; Martin et al., 2014; Rubatto and Angiboust, 2015) fluids that
76 were previously undetectable using bulk methods.

77 Chert and siliceous schist are high- $\delta^{18}\text{O}$ lithologies (Eiler et al., 2001) that are found
78 within the amphibolite-facies Catalina Schist mélangé (Platt, 1975). In this contribution, we
79 explore the metasomatism of a high- $\delta^{18}\text{O}$ garnet- and zircon- bearing metachert from a classic
80 subduction mélangé, in order to better understand the timing and metamorphic conditions of
81 subduction fluid metasomatism, and to gain a more complete picture of how fluids mitigate the
82 influence of high- $\delta^{18}\text{O}$ subduction inputs.

83

84 **CATALINA GARNET QUARTZITE**

85 Although much less numerous than the better-studied garnet-hornblende lithology, tectonic
86 blocks of garnet quartzite are also found within the amphibolite-facies metasedimentary mélangé
87 of the Catalina Schist (Santa Catalina Island, California, USA), as well as in more coherent, fault-

88 bounded sheets (Platt, 1975; Bebout, 1991). In this study, we report on one exceptional sample of
89 garnet quartzite collected from a meter-scale tectonic block hosted in a shale-matrix mélangé from
90 Upper Cottonwood Canyon (33°23'46.20"N, 118°24'52.80"W, Fig. 1A). The quartzite is
91 composed primarily of quartz (93%), garnet (6%), and chlorite (<0.5%), with trace rutile, apatite,
92 amphibole, and zircon (Fig. 1B). Garnet is present in two populations: copious fine-grained
93 (<200µm-diameter) crystals dispersed throughout the sample and a smaller number of larger
94 garnets (1-3mm-diameter, Fig. 1B). The larger crystals have abundant inclusions, which are
95 primarily quartz and apatite. X-ray mapping and major element traverses show that the larger
96 garnets display classic prograde cation-zoning profiles with decreasing Mn and increasing Mg#
97 from core to rim, and with rim compositions similar to smaller, more homogenous (in cations)
98 garnets in the same rock (Figs. 2A, B).

99

100 **Oxygen Isotopes of Quartz and Garnet**

101 Ion microprobe analysis of garnets (Page et al., 2010, see GSA Data Repository for full
102 data, Tables DR-1, DR-2, and methods) shows extreme oxygen isotope zoning; values of $\delta^{18}\text{O}$
103 are 20.8-26.3‰ in garnet cores and 10.0-11.2‰ in garnet rims (Fig. 2A). Both large and small
104 garnets in this sample show a similar range in $\delta^{18}\text{O}$, despite the difference in cation zoning and
105 crystal size. Zoning in oxygen isotopes is sharp, with up to a 7‰ drop in $\delta^{18}\text{O}$ over a few
106 micrometers, whereas cation zonation is much more gradual with slightly increased Ca and Mg
107 in the rims of larger garnets (Fig. 2). Smaller garnets are nearly homogeneous with a slight
108 increase in Mg# from core to rim. Matrix quartz has no systematic zoning in
109 cathodoluminescence imaging (CL) and is homogeneous in $\delta^{18}\text{O}$ with ion microprobe analyses
110 (13.5‰) identical (within uncertainty) to bulk (~2mg) analysis by laser fluorination (13.6‰).

111 Garnet-core and quartz pairs yield reversed fractionations ($\delta^{18}\text{O}_{\text{grt}} > \delta^{18}\text{O}_{\text{qz}}$), indicating profound
112 disequilibrium. Eleven analyses of quartz inclusions in large garnet cores yield $\delta^{18}\text{O} = 13.8$ -
113 16.2% , higher than matrix quartz, but not in equilibrium with host garnet. Inclusions were
114 generally $>50\mu\text{m}$, and commonly along cracks and so are unlikely to preserve their original
115 values.

116

117 **Oxygen Isotopes in Zircon**

118 Zircon was separated from the sample and mounted in epoxy for analysis (see GSA
119 Data Repository). CL imaging (Fig. 3A) reveal oscillatory-zoned cores, often as fragments of
120 crystals, containing inclusions of quartz, K-feldspar, and biotite. These detrital cores are
121 surrounded by annuli of variable intensity, somewhat mottled zircon, containing inclusions of
122 quartz, biotite, sphene, and rutile. Outside of this mottled zone, zircons typically have darker-
123 intensity-CL oscillatory-zoned rims, with rare crystals containing a brighter outer rim with faint
124 oscillatory zoning.

125 Zircon was analyzed for their oxygen isotope ratios by ion microprobe using both a
126 ~ 15 - and a sub- $1\text{-}\mu\text{m}$ diameter beam (Tables DR-4, -5). Highly precise and accurate oxygen
127 isotope ratios from the larger analysis pits are correlated with CL zonation and inclusion
128 population. Zircon cores ($n=7$) have $\delta^{18}\text{O}$ from 4.7 to 8.4‰ (Figs. 3A, 3B). Zircon with mottled
129 CL immediately outside of detrital cores ($n=17$) has an extremely high $\delta^{18}\text{O}$ (Fig. 3A, 3B) of
130 $22.6 \pm 3.3\%$ (2 SD, sample) if one anomalously low analysis is discounted. Intermediate-
131 intensity oscillatory-zoned rims ($n=20$) have lower $\delta^{18}\text{O}$ values ($17.3 \pm 3.9\%$), and rare bright
132 outer rims have lower-still $\delta^{18}\text{O}$ values ($12.9 \pm 3.3\%$). To further determine if there is a
133 systematic zoning pattern in zircon like that found in garnet, 29 sub- $1\text{-}\mu\text{m}$ analyses (following

134 the method of Page et al., 2007) were made in traverses across a single zircon (Fig. 3A). These
135 high-spatial resolution (but less precise, ± 0.9 - 1.7% , 2S.D.) analyses confirm the presence of a
136 low $\delta^{18}\text{O}$ core ($6.3 \pm 1.1\%$, 2S.D., $n=6$), surrounded by an extremely high- $\delta^{18}\text{O}$ mottled CL
137 region ($22.6 \pm 2.4\%$, $n=15$), indistinguishable within the uncertainty of the sub- $1\text{-}\mu\text{m}$ data from
138 the $15\text{-}\mu\text{m}$ -diameter analyses of the same zones. An outer, darker oscillatory-zoned rim has $\delta^{18}\text{O}$
139 of $17.0 \pm 2.5\%$, $n=8$). The zircon chosen for this analysis does not have an outermost, lighter rim.

140

141 **PRESSURE, TEMPERATURE, AND TIME HISTORY**

142 The limited mineralogy of this sample coupled with its metasomatic history and zoned
143 minerals, makes thermobarometry challenging. However, an equilibrium assemblage diagram
144 calculated using an estimate of the bulk composition and the computer package *Perple_X*
145 (Connolly, 2009; Fig. DR-1) yields reasonable results. The observed assemblage (qz+grt+ru±chl)
146 is predicted to form at pressures greater than 8kbar and temperatures greater than 550°C . The
147 core to rim increase of Mg# observed in the large garnets is consistent with growth during
148 increasing temperatures in the presence of chlorite, and is predicted by the model to have taken
149 place at ~ 550 - 650°C , at pressures of greater than 11kbar, consistent with existing pressure and
150 temperature estimates of amphibolite blocks in the same *mélange* and [Zr]-in-rutile thermometry
151 from this same sample (Sorenson and Barton, 1987; Hartley et al., 2016; Penniston-Dorland et
152 al., 2018). The closeness between the conditions predicted by the model and existing
153 thermobarometry from Catalina suggests that the metasomatism of this block did not involve
154 substantial change in cation composition. Regardless of the precise conditions of metamorphism,
155 the concomitant decrease in $\delta^{18}\text{O}$ with increasing Mg# in garnet requires metasomatism as the
156 sample increased in temperature within the subduction environment.

157 Zircons were additionally analyzed by SHRIMP-RG for U-Pb isotopes and select trace
158 elements (GSA Data Repository). Detrital zircon cores have more elevated Th/U ratios (0.36-
159 0.89), and are older than rims; 8 of 9 analyses yield a coherent ^{204}Pb -corrected $^{206}\text{Pb}^*/^{238}\text{U}$ age of
160 124.6 +1.4/-2.9 Ma (Fig. 3C). Th/U ratios of rims are lower (0.02-0.13) and yield an age of
161 115.1±2.4 Ma consistent with an igneous origin for zircon cores, and a metamorphic one for the
162 rims (Fig. 3C). Zircon rims also have smaller Eu-anomalies (Eu/Eu* close to 1) and flatter
163 HREE patterns, consistent with a metamorphic origin in a garnet-present, plagioclase-absent
164 high-pressure environment (Fig. 3D).

165

166 **DISCUSSION**

167 Taken together, the P-T-t-fluid data preserved in garnet and zircon from this sample
168 provide a detailed record of metasomatic events within the subduction channel. A mixed-
169 lithology protolith containing both extremely high- $\delta^{18}\text{O}$ siliceous material intermixed with
170 intermediate/mafic igneous material including detrital igneous zircon grains was subducted in the
171 Catalina trench. The most plausible interpretation is that the protolith was a mixture of chert or
172 siliceous ooze mixed with ~124 Ma arc volcanoclastic material. The relative purity of the
173 quartzite and the narrow range of zircon core ages seems to preclude weathering of plutonic
174 source material as an origin for the inherited cores. This mixed sediment was subducted and
175 metamorphosed initially as a closed system, with larger, prograde garnet cores having high and
176 unchanging $\delta^{18}\text{O}$ values. The extreme oxygen isotope ratio of this sample (quartz in equilibrium
177 with garnet cores at 550°C would have been greater than 30‰, Valley et al., 2003) makes it
178 highly sensitive to infiltration from external fluids with lower $\delta^{18}\text{O}$. A second generation of
179 garnets nucleated near the peak of metamorphism, but their growth was not initiated by an

180 external fluid, as core $\delta^{18}\text{O}$ compositions are identical to larger garnets. As metamorphic
181 temperatures reached their peak, an external fluid permeated the sample, perhaps due to
182 introduction of the block into the subduction mélange, shifting matrix quartz $\delta^{18}\text{O}$ from $\sim 30\text{‰}$ to
183 13.6‰ . Slow rates of intragranular diffusion preserve a record of the original high- $\delta^{18}\text{O}$
184 composition of garnet and zircon, and their continued growth documents decreasing $\delta^{18}\text{O}$ from
185 $\sim 24\text{‰}$ to $\sim 17\text{‰}$ to $\sim 11\text{‰}$ VSMOW, possibly in two discreet pulses. Fractionation between
186 matrix quartz and garnet rim compositions yield temperatures of $\sim 600\text{--}750^\circ\text{C}$ (Valley et al.,
187 2003), consistent with estimates of peak metamorphic temperatures for the block and the region.
188 Likewise, garnet cation composition records increasing temperature (pressure is not well
189 constrained) during metasomatism. Perhaps upwelling within the subduction channel stopped
190 quartz recrystallization and garnet growth simultaneously, effectively ending the record
191 preserved in this sample.

192 The limited range of $\delta^{18}\text{O}$ in quartz and calcite veins within the Catalina Schist first
193 reported by Bebout and Barton (1989) suggests that the entire package of subduction rocks on
194 Catalina Island interacted with a remarkably homogeneous supracrustal fluid reservoir derived
195 from metamorphic dehydration of minerals deeper along the subducting slab with an oxygen
196 isotope composition of $13 \pm 1.0\text{‰}$ VSMOW. The quartz $\delta^{18}\text{O}$ value for the block in mélange in
197 this study (13.6‰ VSMOW) yields a calculated water $\delta^{18}\text{O}$ value of 12.3‰ VSMOW (650°C ,
198 Friedman and O'Neil, 1977) in close agreement with the range reported by Bebout and Barton.

199 Although high- $\delta^{18}\text{O}$ sediments make up a volumetrically small portion of subducted
200 material, the extreme contrast between their isotope ratios and those of the mantle make them
201 likely candidates for introducing fine-scale isotope anomalies in the sub-arc mantle. Indeed, the
202 recent discovery of high- $\delta^{18}\text{O}$ S-type granite within supra-subduction-zone mantle as well as

203 this contribution show that this can happen (Spencer et al., 2017). The sample documented in this
204 study is an example of the most extreme contrast in $\delta^{18}\text{O}$ that one might expect to be subducted,
205 with an estimated protolith $\delta^{18}\text{O}$ of 30‰. However, the metasomatic processes documented by
206 garnet and zircon zonation in this metachert from Catalina show that subduction fluids can all
207 but wipe out extremely high- $\delta^{18}\text{O}$ inputs to subduction zones. Given the modest modal
208 proportion of garnet (7%) with respect to quartz (93%) in this sample, and assuming $\delta^{18}\text{O}$ values
209 of 24‰ for garnet and 14‰ for quartz, the whole rock $\delta^{18}\text{O}$ of this rock must be less than 15‰,
210 a value that can also be found in the much more abundant subducted metabasalts with protoliths
211 enriched in ^{18}O by low-temperature interaction with sea water (Eiler, 2001). Subduction fluids
212 play a vital role in the generation of arc magmatism and continental growth, but it also seems
213 that they play an important role in buffering the $\delta^{18}\text{O}$ of rocks that are recycled into the mantle
214 by subduction, with only strongly refractory (and volumetrically minor) phases such as zircon
215 and garnet able to carry extreme oxygen isotope ratios into the mantle.

216

217 **ACKNOWLEDGMENTS**

218 We thank Eric Essene, who provided mentorship, assistance in the field, and partial
219 funding for SIMS analysis, S. Penniston-Dorland, E. Walsh and the 2012 Keck Catalina Project
220 (NSF-REU-1062720) students for assistance with fieldwork on Catalina Island, and the Catalina
221 Island Conservancy for access and field support. Comments from Christopher Spencer, two
222 anonymous reviewers and editor Chris Clarke improved this manuscript and are gratefully
223 acknowledged. Assistance with EPMA and laser fluorination analyses were provided by G.
224 Moore (University of Michigan) and Mike Spicuzza (University of Wisconsin). The WiscSIMS
225 ion microprobe laboratory is supported by National Science Foundation (EAR-1355590,

226 1658823) and the University of Wisconsin–Madison. FZP, EMC, CMF and JWD gratefully
227 acknowledge financial support from Oberlin College and NSF (EAR-1249778). JWV is
228 supported by NSF (EAR-1524336).

229 **REFERENCES CITED**

- 230 Bebout, G. E., 1991, Field-based evidence for devolatilization in subduction zones: implications
 231 for arc magmatism: *Science*, v. 251, p. 413-416.
- 232 Bebout, G. E., and Barton, M. D., 1989, Fluid flow and metasomatism in a subduction zone
 233 hydrothermal system: Catalina Schist terrane, California: *Geology*, v. 17, p. 976-980.
- 234 Bebout, G. E., and Penniston-Dorland, S. C., 2016, Fluid and mass transfer at subduction
 235 interfaces—The field metamorphic record: *Lithos*, v. 240-243, p. 228–258, doi:
 236 10.1016/j.lithos.2015.10.007.
- 237 Connolly, J. A. D. (2009) The geodynamic equation of state: what and how: *Geochemistry,*
 238 *Geophysics, Geosystems*, v. 10:Q10014, doi:10.1029/2009GC002540.
- 239 Cruz-Uribe, A.M., Marschall, H.R., Gaetani, G.A., and Le Roux, V., 2018, Generation of
 240 alkaline magmas in subduction zones by partial melting of mélange diapirs—An
 241 experimental study: *Geology*, v. 46, p. 343–346, doi: 10.1130/G39956.1.
- 242 Eiler, J.M., 2001, Oxygen isotope variations of basaltic lavas and upper mantle rocks, *in* Valley,
 243 J.W. and Cole, D.R. eds., *Reviews in Mineralogy & Geochemistry Vol. 43: Stable Isotope*
 244 *Geochemistry: Mineralogical Society of America*, p. 319–364,
 245 <https://doi.org/10.2138/gsrng.43.1.319>.
- 246 Eiler, J.M., McInnes, B., Valley, J.W., Graham, C.M., and Stolper, E.M., 1998, Oxygen isotope
 247 evidence for slab-derived fluids in the sub-arc mantle: *Nature*, v. 393, p. 777–781,
 248 <https://doi.org/10.1038/31679>.
- 249 Eiler, J.M., Schiano, P., Kitchen, N., and Stolper, E.M., 2000, Oxygen-isotope evidence for
 250 recycled crust in the sources of mid-ocean-ridge basalts: *Nature*, v. 403, p. 530–534,
 251 <https://doi.org/10.1038/35000553>.
- 252 Friedman, I. and O’Neil, J. R., 1977, Compilation of stable isotope fractionation factors of
 253 geochemical interest: U.S. Geological Survey Professional Paper, v. 440-KK.
- 254 Hartley, E.S., Pereira, I., Moreira, H., Page, F.Z., and Storey, C.D., 2016, Petrology and trace
 255 element thermometry of garnet-quartzite from the Catalina Schist, *Geological Society of*
 256 *America Abstracts with Programs*, v.48, n.7. Abst. 258-3.
- 257 Hickmott, D., Sorensen, S. S., and Rogers, P., 1992, Metasomatism in a subduction complex;
 258 constraints from microanalysis of trace elements in minerals from garnet amphibolite from
 259 the Catalina Schist: *Geology*, v. 20, p. 347–350.
- 260 King, R. L., Bebout, G. E., Moriguti, T., and Nakamura, E., 2006, Elemental mixing systematics
 261 and Sr-Nd isotope geochemistry of melange formation: Obstacles to identification of fluid
 262 sources to arc volcanics: *Earth and Planetary Science Letters*, v. 246, p. 288–304.
- 263 Kolodny, Y., and Epstein, S., 1976, Stable isotope geochemistry of deep sea cherts: *Geochimica*
 264 *et Cosmochimica Acta*, v. 40, p. 1195-1209.
- 265 Marschall, H.R., and Schumacher, J.C., 2012, Arc magmas sourced from mélange diapirs in
 266 subduction zones: *Nature Geoscience*, v. 5, p. 862–867, doi: 10.1038/ngeo1634.
- 267 Martin, L.A., Rubatto, D., Crépisson, C., Hermann, J., Putlitz, B., and Vitale Brovarone, A.,
 268 2014, Garnet oxygen analysis by SHRIMP-SI: Matrix corrections and application to high-
 269 pressure metasomatic rocks from Alpine Corsica: *Chemical Geology*, v. 374-375, p. 25–36,
 270 doi: 10.1016/j.chemgeo.2014.02.010.
- 271 Page, F. Z., Ushikubo, T., Kita, N. T., Riciputi, L. R., and Valley, J. W., 2007, High-precision
 272 oxygen isotope analysis of picogram samples reveals 2 μm gradients and slow diffusion in
 273 zircon: *American Mineralogist*, v. 92, p. 1772-1775.

274 Page, F. Z., Kita, N. T., and Valley, J. W., 2010, Ion microprobe analysis of oxygen isotopes in
275 garnets of complex chemistry: *Chemical Geology*, v. 270, p. 9-19.

276 Page, F.Z., Essene, E.J., Mukasa, S.B., and Valley, J.W., 2014, A garnet-zircon oxygen isotope
277 record of subduction and exhumation fluids from the Franciscan Complex, California:
278 *Journal of Petrology*, v. 55, p. 103–131.

279 Payne, J.L., Hand, M., Pearson, N.J., Barovich, K.M., and McInerney, D.J., 2015, Crustal
280 thickening and clay: Controls on O isotope variation in global magmatism and siliciclastic
281 sedimentary rocks: *Earth and Planetary Science Letters*, v. 412, p. 70–76, doi:
282 10.1016/j.epsl.2014.12.037.

283 Penniston-Dorland, S. C., Bebout, G. E., Pogge von Strandmann, P. A. E., Elliott, T., and
284 Sorensen, S. S., 2012, Lithium and its isotopes as tracers of subduction fluids and
285 metasomatic processes: Evidence from the Catalina Schist, California, USA: *Geochimica et*
286 *Cosmochimica Acta*, v. 77, p. 530-545.

287 Penniston-Dorland, S. C., Gorman, J. K., Bebout, G. E., Piccoli, P. M., and Walker, R. J., 2014,
288 Reaction rind formation in the Catalina Schist: Deciphering a history of mechanical mixing
289 and metasomatic alteration: *Chemical Geology*, v. 384, p. 47–61.

290 Penniston-Dorland, S.C., Kohn, M.J., and Piccoli, P.M., 2018, A mélange of subduction
291 temperatures: Evidence from Zr-in-rutile thermometry for strengthening of the subduction
292 interface: *Earth and Planetary Science Letters*, v. 482, p. 525–535, doi:
293 10.1016/j.epsl.2017.11.005.

294 Platt, J., 1975, Metamorphic and deformational processes in the Franciscan Complex, California:
295 some insights from the Catalina Schist terrane: *Bulletin of the Geological Society of*
296 *America*, v. 86, p. 1337–1347.

297 Rubatto, D., and Angiboust, S., 2015, Oxygen isotope record of oceanic and high-pressure
298 metasomatism: a P–T–time–fluid path for the Monviso eclogites (Italy): *Contributions to*
299 *Mineralogy and Petrology*, v.170:44, p. 1–16, doi: 10.1007/s00410-015-1198-4.

300 Russell, A. K., Kitajima, K., Strickland, A., Medaris, Jr, L. G., Schulze, D. J., and Valley, J.W.,
301 2013, Eclogite-facies fluid infiltration: constraints from $\delta^{18}\text{O}$ zoning in garnet: *Contributions*
302 *to Mineralogy and Petrology*, v. 165, p. 103-116.

303 Spencer, C.J., Cavosie, A.J., Raub, T.D., Rollinson, H., Jeon, H., Searle, M.P., Miller, J.,
304 McDonald, B.J., Evans, N.J., and EIMF, 2017, Evidence for melting mud in Earth’s mantle
305 from extreme oxygen isotope signatures in zircon: *Geology*, v. 45, p. 975-978, doi:
306 10.1130/G39402.1.

307 Valley, J. W., 2003, Oxygen isotopes in zircon: *Reviews in Mineralogy and Geochemistry*, v. 53,
308 p. 343-385.

309 Vielzeuf, D., Veschambre, M., and Brunet, F., 2005, Oxygen isotope heterogeneities and
310 diffusion profile in composite metamorphic-magmatic garnets from the Pyrenees: *American*
311 *Mineralogist*, v. 90, p. 463–472.

312

313

314 **FIGURE CAPTIONS**

315 Figure 1. A) Geologic sketch map of Santa Catalina Island, California (after Platt, 1975) showing
316 sample locations. B) Polished thick section of a garnet quartzite showing two garnet sizes. (grt1
317 – larger, cation-zoned garnet, grt2 – smaller, garnet crystals, homogeneous in cations, qz-quartz,
318 ru – rutile, ap – apatite, chl – chlorite)

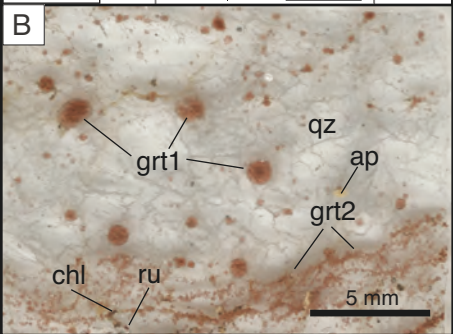
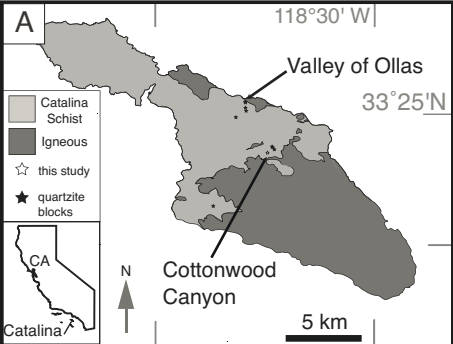
319

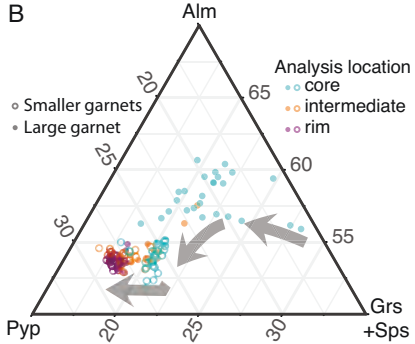
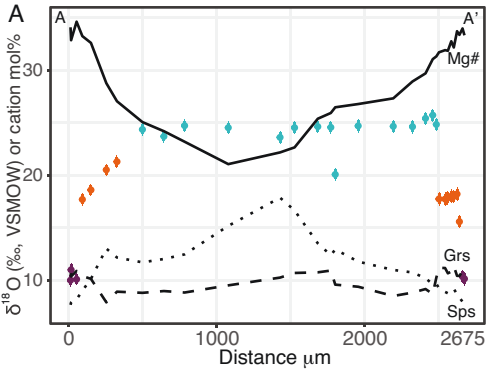
320 Figure 2. A) $\delta^{18}\text{O}$ and cation traverse, rim to rim, of a single $\sim 2.5\text{mm}$ dia. garnet. The core region
321 is generally homogeneous at $\sim 25\text{‰}$ (aquamarine points), transitions to intermediate values
322 (orange) and low, $\sim 10\text{‰}$ rims (purple) over short intervals, although zoning is asymmetric.

323 $\text{Mg}/(\text{Mg}+\text{Fe})$ ($\text{Mg}\#$, solid line) increases continuously core to rim. B) Ternary diagram of garnet
324 cation compositions, mm-scale garnets are shown as solid circles, $\sim 100\mu\text{m}$ -scale garnets shown
325 as open circles. Analysis location (core, intermediate, rim) is also correlated with $\delta^{18}\text{O}$, and
326 indicated by color, as in A. Larger garnets have greater cation zoning than smaller garnets
327 (dashed arrow), and all oxygen isotope zonation takes place at the most pyrope-rich
328 compositions for both sizes (alm - almandine, pyp – pyrope, grs -- grossular, sps – spessartine).

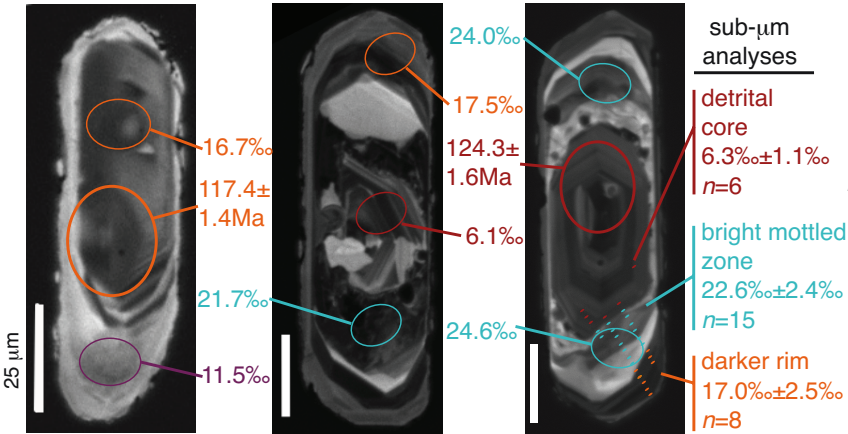
329

330 Figure 3. Catalina quartzite zircon chemistry and age A) CL images ($25\mu\text{m}$ scale bars) of three
331 zircons showing different CL domains (see text for details). Analysis of $\delta^{18}\text{O}$ are shown with two
332 spot sizes and labeled with values in VSMOW ($\sim 15\mu\text{m}$, $\pm 0.2\text{-}0.4\text{‰}$ 2S.D., Table DR-5; $< 1\mu\text{m}$, \pm
333 2.5‰ 2S.D., Table DR-6). B) Histogram of analyses of zircon and garnet with a $15\mu\text{m}$ diameter
334 spot from sample 05C-09 grouped by CL domain and/or location across a traverse, colors as in
335 Figure 2.





A



B

